Unsupervised Saliency Detection in 3D video based on Multi-scale Segmentation and Refinement

Ping Zhang*, Pengyu Yan, Jiang Wu, Jingwen Liu, Fengcan Shen

***Abstract*—In this paper, we propose an unsupervised salient object detection method in 3D videos. Both temporal and depth information are efficiently considered, and multi-scale architecture and graph-based refinement are built to improve accuracy and robustness. Firstly, the input video frame is segmented into non-overlapping superpixels by combining both appearance and depth information at the input. A multi-scale architecture is also deployed after the segmentation with different segmentation parameters. Secondly, the initial saliency score of each segmented superpixel in each scale is calculated via global contrast which is defined by appearance, depth, and motion cues from two consecutive frames. Thirdly, the initial saliency in each scale is refined by smoothing over graphs built by three spatial-temporal feature priors-color, depth and motion. Finally, the result is obtained by fusing three refined saliency maps in three scales. The experiments on two widely-used datasets illustrate that our method outperforms state-of-the-art algorithms in terms of accuracy, robustness, and reliability.**

***Index Terms*—Saliency detection, Segmentation, Multi scale, Appearance, Motion, Depth, Graphical model**

I. INTRODUCTION

Human visual attention is most significant in human visual system, as it ensures us to pop out the most important object in a complex scene.

In 1998, Itti [1] defined “saliency” as the area which is much different from the surrounding. This definition was broadly accepted by the research community. Later, based on such definition, lots of method like [2]–[7] were developed to improve the performance of saliency detection in static color image. In 2015, Gong et al. [8] designed a saliency model based on novel propagation algorithm employing the teaching-to-learn and learning-to-teach strategies to process the complex regions. Similarly, emphasizing the entire object, Fu et al. [9] utilized normalized graph cut to extract the saliency area.

With the development of the 3D measuring device, depth information is naturally incorporated in the saliency detection model. Zhang et al. [10] used appearance, depth, motion, illumination and direction to calculate bottom-up saliency in an image. In [11], depth is used to weigh the 2D saliency result. Based on that, Niu [12] constructed a depth weight curve by assuming that the comfort zone and popping out object are more salient than any other region or object. In [13], [14], instead of using depth as a weight bias, the authors considered it as another feature and calculated the depth-only saliency map via global contrast. In [15], based on appearance and depth information from images, bootstrap learning and multiscale fusion are designed to obtain comprehensive saliency result.

Since human visual attention is easily draw by the fast moving objects, the spatial-temporal information between video frames could help improve accuracy of saliency detection. In [10], [16], a saliency detection method was proposed to fuse spatial, motion and depth saliency maps to yield the final saliency map. In [17], motion and color histogram are extracted at superpixel level as local features and at frame level as global features to obtain the saliency result. In [18], [19], a graph considering spatial-temporal features between video frames was built to generate saliency maps. In 2018, Zhou et al. [20] used localized estimation and spatialtemporal refinement to pop out the salient object in videos.

The success of convolutional neural networks (CNN) [21] in ImageNet2012 competition [22] showed that deep neural nets have advantages on feature utilizing. Li et al. [23] used CNN to extract multi-scale features from image to obtain saliency result. In 2015, Zhao et al. [24] calculated the saliency via high-level feature, which is obtained through CNN networks. Later, considering the temporal information from videos, [25] used two consecutive frames as the input of the fully convolutional networks to obtain spatialtemporal saliency.

Although there are many existed methods about saliency detection, very few of them efficiently exploited both depth and temporal information from video sequences. Besides, they are limited in preserving a clear edges of the foreground object when considering for a wide range of 3D video. As for deep-learning methods, they need quantities of data and supervised training to achieve good performance.

In order to overcome aforementioned challenges, as shown in Fig. 1, we propose a 3D video saliency detection method considering appearance, depth and temporal information from sequences. Multi-scale architecture, initial saliency calculation via global contrast and refinement based on graphical model are deployed. The contributions are concluded as following:

- We upgrade the SLIC algorithm by adding depth information and build an multi-scale architecture after segmentation with different parameters. Adding depth information could make segmentation result with a well preserved shape and edge, while multi scales improve the robustness.
- We build a graphical model to refine the initial saliency map, which is obtained via appearance, depth and motion

This research is supported by the Science and Technology Planning Project of Sichuan Province, China (No. 2018GZ0166), National Natural Science Foundation of China (No. 61308102). (Corresponding author: Ping Zhang.)

The authors are with the School of Optoelectronic Science and Engineering, University of Electronic Science and Technology of China, Chengdu 610054, China (e-mail: pingzh@uestc.edu.cn, py.yan965@gmail.com, 1625523461@qq.com, 18702505013@163.com, xiaoshenrobert@outlook.com)

from frames. Leveraging each feature prior to refine the initial saliency map improves the features' utilizing efficiency and prompts a clear background and well-preserved foreground.

II. Proposed Method

A. Segmentation with multi-scale

1) Upgraded SLIC Model: In this part, our aim is to decompose the input image into non-overlapping superpixels and preserve accurate object's shape and edge. While the traditional K-means algorithm in SLIC only used appearance and distance to cluster pixels, we further add depth information with appropriate weight. We set the depth feature distance as $D_d = \sqrt{(d_j - d_i)^2}$, where d_j and d_i represent the j^{th} and i^{th} superpixels' depth value, respectively. By giving a weight to depth feature distance as β, the complete feature distance evaluation becomes:

$$D' = (1-\beta)D_c + \beta D_d \tag{1}$$

$$D = \sqrt{(\frac{D'}{m})^2 + (\frac{D_S}{S})^2} \tag{2}$$

Here, D' is the weighted mean of color and depth feature distance. D_c and D_S are the Euclidean distance of color and space. m is a parameter related to the largest color distance in one image and S is the expected number of superpixel. Throughout the experiment, β and m are set to 0.5 and 15, as they give the best segmentation performance.

2) Multi-scale Architecture: In segmentation, small number of superpixels reduces the ability to preserve accurate edges of objects, while large number of superpixels misses objects' important corners. Furthermore, the number of optimal superpixels depends on each input frame.

In order to increase the robustness of the proposed algorithm, a Multi-scale approach is integrated with the SLIC algorithm. The first part of Fig. 1 shows the modified SLIC algorithm's output for a image with appearance and depth information and segmented to 200, 600 and 1000 superpixels. The feature value in each superpixel is the mean of all pixel's feature value in the superpixel area.

The remaining part of the model is calculated upon superpixel and scale level. At the last step, the results of all scales are fused using the designed way described in Section II-D.

B. Initial Saliency

In this part, within superpixel level, two steps are proposed to calculate the initial saliency map.

First, since L-a-b color correlates better to the perceptual of human eyes, we use CIE-Lab color space to represent the appearance of input image. Then, motion is calculated by the TV-L_1 Optical Flow [26], [27], and the two parameters of motion, v_x and v_y, can be obtained by solving the equation $I(x, y, t) = I(x + \mathrm{d}x, y + \mathrm{d}y, t + \mathrm{d}t)$, constraint by $I_x v_x + I_y v_y + I_t = 0$. I is the luminance.

Second, we use global contrast with color, depth, motion and spatial distance to generate the initial saliency maps. We use arithmetic mean of color, motion and depth of all

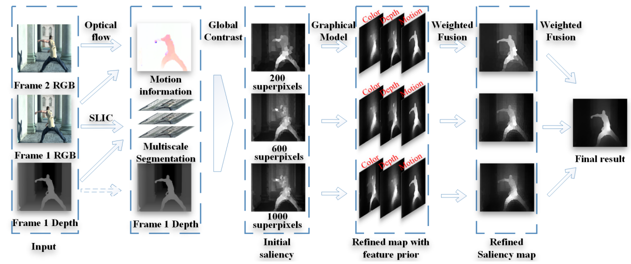

Fig. 1: Flowchart of the proposed method

pixels in each superpixel area to represent the feature value of whole superpixel. The spatial distance is calculated among the barycenters of superpixels, and each feature distance is calculated by Euclidean distance:

$$d_C(R_j, R_i) = \sqrt{(L_{R_j} - L_{R_i})^2 + (a_{R_j} - a_{R_i})^2 + (b_{R_j} - b_{R_i})^2} \tag{3}$$

$$d_M(R_j, R_i) = \sqrt{(v_{x_{R_j}} - v_{x_{R_i}})^2 + (v_{y_{R_j}} - v_{y_{R_i}})^2} \tag{4}$$

$$d_D(R_j, R_i) = \sqrt{(D_{R_j} - D_{R_i})^2} \tag{5}$$

where R_i denotes the i^{th} superpixel, and L, a, b are the color values under CIE-Lab. d_C, d_M and d_D are the feature distance of color, motion and depth, respectively.

After the feature distance calculation, according to the visual mechanism of human where the closer the two superpixels are, the more influence they had for each other, we designed the weight coefficient based on spatial distance as follows:

$$\omega(R_j, R_i) = \exp(-\frac{d_S(R_j, R_i)}{\sigma}) \tag{6}$$

where d_S represents the spatial distance among the barycenter of the superpixels. The value of the parameter σ is 0.6.

Using weight coefficient, we can obtain the score of each superpixel under each feature:

$$\begin{aligned} S_F(R_i) &= \sum_{R_j \in \Omega} s_F(R_j, R_i) \\ &= \sum_{R_j \in \Omega} \omega(R_j, R_i) \cdot d_F(R_j, R_i) \end{aligned} \tag{7}$$

where the notation "F" stands for either "C","M" or "D", *i.e.*, color, motion, and depth, correspondingly. s_F is weighted "F" feature distance between two superpixels and $S_F(R_i)$ is the saliency score of R_i^{th} superpixel under "F" feature. Ω is the set of all the superpixels in one frame.

By normalizing all superpixels' score, the "F" feature saliency map is obtained. Then, we calculate the aggregation degree as the evaluation weight to fuse all feature saliency maps:

$$\mu_F = \frac{\sum\limits_{R_i \in \Omega} \sqrt{(y_{R_i} - \overline{p_{y_F}})^2 + (x_{R_i} - \overline{p_{x_F}})^2} \cdot S_F(R_i)}{\sum\limits_{R_i \in \Omega} S_F(R_i)} \tag{8}$$

$$S = \frac{\sum_{F \in \{C,M,D\}} 1/\mu_F \times S_F}{3} \tag{9}$$

where "F" means this equation is used to calculate value of "F" feature saliency map. (x_{R_i}, y_{R_i}) is the coordinate barycenter of the R_i^{th} superpixel, $(\overline{p_{x_F}}, \overline{p_{y_F}})$ is the barycenter of the saliency area calculated by saliency scores of all superpixels, and μ_F is the aggregation degree of each feature saliency map. $S_F(R_i)$ is the "F" feature saliency score of R_i^{th} superpixel. S is the initial saliency map.

C. Saliency refinement based on Graphical Model

Initial saliency map obtained from global contrast has many artifacts at object's edge and nearby background, as seen in Fig. 2(a). To regularize salient object's shape and clean nearby background, a refinement based on graphical model is proposed. A probability transition function could reduce the negative impact between the salient superpixel and nearby non-salient superpixel, and balance the relationship among homogeneous salient superpixel. Thus, the saliency score of superpixels in background would be decreased, which helps prompt a clear background and well-preserved object.

First, upon initial saliency maps, we separately use motion, color and depth features to calculate the transition probability $P_{R_j,R_i,F}$:

$$P_{R_j,R_i,F} = \frac{W_{R_i,R_j,F}}{\sum_{R_j \in \Omega_{R_i}} W_{R_i,F}} \tag{10}$$

where $F \in \{C, M, D\}$, and $W_{R_i,R_j,F} = \exp(-\frac{d_F(R_j,R_i)}{\sigma})$. We observe that the more different the two superpixels feature is, the smaller the transition probability would be.

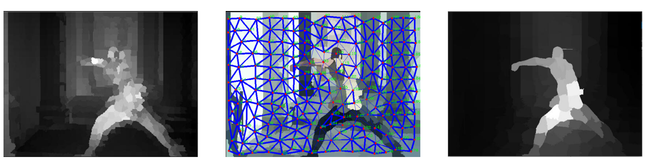

(a) Initial Saliency (b) Graphical Model (c) Optimized Saliency

Fig. 2: Optimization based on Graphical Model

Based on the transition probability, we draw the lines among the superpixels' barycenters and use the thickness of the lines to represent the value of transition probability. If the feature contrast of these two superpixels are small, the line would be thick, and vice versa (Fig. 2(b)). In Fig. 2(b), the rough outline of the objects could be presented by the thin lines, which reflect a big difference between the objects and the background. It is also the location where the line just cross the objects' edge.

Second, we use the transition probability as the weight to process the initial saliency maps:

$$U_F = \sum_{R_j,R_i \in \Omega} P_{R_j,R_i,F} \cdot s(R_j, R_i) \tag{11}$$

where $s(R_j, R_i)$ means the fused feature distance between two superpixels implied in the initial saliency maps and it can be calculated from eq. (7) and eq. (8) by $s(R_i, R_j) = \frac{1}{3}\sum_{F \in C,M,D} \frac{1}{\mu_F} s_F(R_j, R_i)$.

From this equation, we can gain the refined saliency map by each feature prior, for example U_M represents the refined saliency map by motion prior.

Third, after the normalization, the three refined saliency maps by three features priors would be fused:

$$U = \frac{1}{3}\sum_{F \in \{C,M,D\}} U_F. \tag{12}$$

The refined saliency maps are with well-preserved object's shape and edge, as shown in Fig. 2(c).

D. Fusion of Multi-scale Saliency Maps

After section II-C, there are three refined saliency maps under three scales. We name each saliency map as U_n, *e.g.*, U_1 means the saliency map in the first scale.

$$U_A = \frac{1}{3}\sum_{n=1}^{3} U_n + \prod_{n=1}^{3} U_n. \tag{13}$$

In order to combine the advantages of each scale, we develop a fusing method by combining an average sum and a multiplication. In the sum part, we average the sum to make the saliency value of each superpixel still between $[0, 1]$. In the multiplication part, we multiple saliency maps together. The common saliency areas in all saliency maps would be enlarged, and the non-common saliency area or common none saliency area in all saliency maps would be greatly diminished (because it is the multiply between 0 and 1). In multiplication part, the saliency value of each superpixel is among $[0, 1]$ as well. The final result is obtained after normalization of U_A.

III. Experiments and Evaluation

In this section, two steps are adapted to evaluate our experiment with two public 3D video sequence datasets, which are 3D-HEVC [28] and NAMA3DS1 [29]. The first step is to vindicate every part of our proposal is rational and necessary. The second step is to compare our method with other state-of-the-art methods.

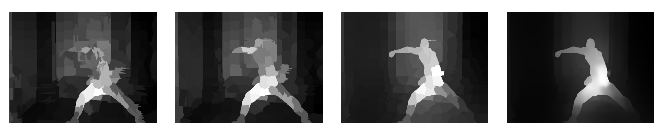

Fig. 3: the images from left to right are:initial saliency map without depth, initial saliency map with depth, refining based on graphical model, result of multi-scale approach

A. Vindication of Proposal

From Fig. 3, by comparing the result of each step in our approach, the importance of each step in our proposal is presented. As the first two sub-images in Fig. 3 shows, adding depth could help to improve the performance of the segmentation and initial saliency maps. After refinement, the quality of the saliency maps improves significantly, which preserved the object edge and regularized the object shape. The multi-scale approach further improves the saliency result in the last subfigure as shown in Fig. 3.

B. Comparison with other Methods

In the next experiments, we compare our proposal with thirty state-of-the-art saliency detection methods: ITTI [1], GBVS [30], FT [31], MR [7], SPL [32], MDF* [23], RFCN* [33], RGBD [14], WANG2DV [34], FCN* [25],

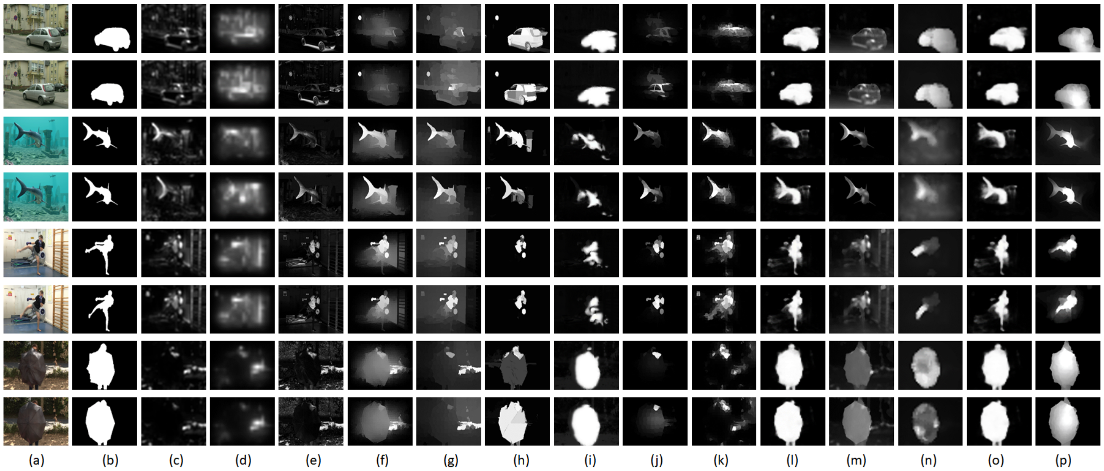

Fig. 4: Example of saliency results of differen methods. (a) Original frame. (b) Ground Truth. (c)-(O) Results of ITTI [1], GBVS [30], FT [31], MR [7], SPL [32], MDF* [23], RFCN* [33], RGBD [14], WANG2DV [34], FCN* [25], ZHANG3DV [10], LINO3DV [16] and FCN-D* [25]. (p) Our proposal

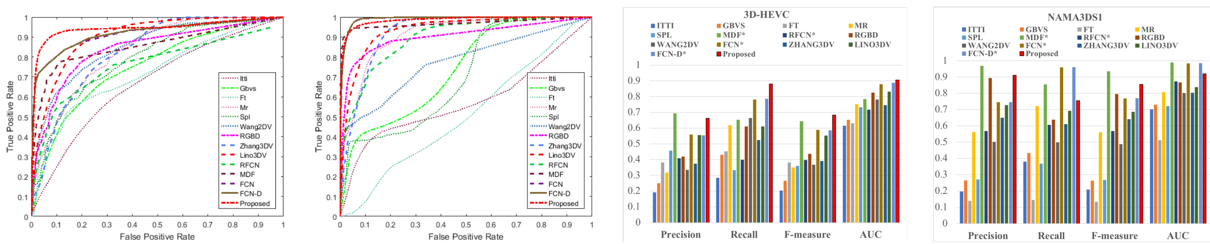

Fig. 5: Evaluation. From left to right: ROC on 3D-HEVC and NAMA3DS1, and chart on 3D-HEVC and NAMA3DS1

TABLE I: Measurement

Type		2D							3D	2DV		3DV			
Datasets	Models	ITTI	GBVS	FT	MR	SPL	MDF*	RFCN*	RGBD	WANG2DV	FCN*	ZHANG3DV	LINO3DV	FCN-D*	Proposed
3D-HEVC	Precision	0.1926	0.2496	0.3815	0.3180	0.4567	0.6938	0.4086	0.4192	0.3350	0.5595	0.3745	0.5562	0.5546	0.6626
	Recall	0.2846	0.4303	0.4521	0.6191	0.3331	0.6533	0.3993	0.6109	0.6637	0.7811	0.5249	0.6112	0.7856	0.8802
	F-measure	0.2027	0.2660	0.3825	0.3506	0.3594	0.6438	0.3968	0.4367	0.3684	0.5888	0.3908	0.5527	0.5849	0.6821
	AUC	0.6157	0.6526	0.6314	0.7521	0.7336	0.7840	0.7178	0.8251	0.7811	0.8792	0.7463	0.8318	0.8886	0.9057
NAMA3DS1	Precision	0.1981	0.2655	0.1392	0.5633	0.2720	0.9688	0.5681	0.8943	0.5017	0.7455	0.6509	0.7277	0.7454	0.9114
	Recall	0.3804	0.4336	0.1456	0.7224	0.3681	0.8548	0.6067	0.6382	0.4988	0.9604	0.6115	0.6929	0.9616	0.7556
	F-measure	0.2095	0.2643	0.1331	0.5611	0.2684	0.9353	0.5684	0.7967	0.4887	0.7696	0.6409	0.6863	0.7697	0.8553
	AUC	0.7017	0.7305	0.5129	0.8077	0.7225	0.9901	0.8727	0.8667	0.8022	0.9848	0.8033	0.8380	0.9851	0.9197

ZHANG3DV [10], LINO3DV [16] and FCN-D* [25], where the proposals with '*' are deep-learning based method. In order to conduct the experiments more convincingly, we slightly modified FCN deep-learning method by guiding the origin saliency results with depth maps to form it into a '3D video based' method, named as FCN-D.

TABLE II: Time Consuming Evaluation

Models	ITTI	GBVS	FT	MR	SPL	MDF*	RFCN*
Time Cost	0.23 s	0.17 s	0.21 s	1.53 s	3.38 s	81.23 s	28.49 s
Models	RGBD	WANG2DV	FCN*	ZHANG3DV	LINO3DV	FCN-D*	Proposed
Time Cost	1.71 s	2.34 s	0.7 s	7.82 s	5.35 s	1.3 s	26.37 s

The qualitative comparisons are presented in Fig. 4, which consists four pairs of two consecutive frames-two pairs are from 3D-HEVC and the other two pairs are from NAMA3DS1, and the results shows that our proposed method achieves the best visual effects. The ROC curves and the chart of measures' value on two datasets are draw in Fig. 5. Detailed evaluation measures, including precision, recall, F-measure and AUC, are presented in Table I. From the results, it could conclude that our method outperforms all other methods on the first datasets and exceeds all traditional methods on the second datasets. However, due to the weak depth maps in the second datasets, our method yield an almost same but slightly poor results compared with three deep-learning methods. Nevertheless, compared with deep-learning saliency detection, our method is unsupervised and no need of quantitative manufactured datasets. Our proposal is implemented by using C++ with OpenCV 3 in a desktop with i7-6700K and 16GB RAM and it costs 26.37 s to obtain a saliency image from video frames. The time cost comparisons with the state-of-the-art methods are shown in Table II.

IV. Conclusion

In this paper, we improved the SLIC algorithm and build an multi-scale architecture based on segmentation. Additionally, refining method based on graphical model is adopted to improve the object's shape and edge in the saliency maps. The experiments on 3D-HEVC and NAMA3DS1 datasets verify the excellent performance of our proposal. The saliency maps using the proposed method consist of objects with clear shape and edge, demonstrating robustness of the proposed algorithm.

REFERENCES

[1] L. Itti, C. Koch, and E. Niebur, "A model of saliency-based visual attention for rapid scene analysis," *IEEE Transactions on Pattern Analysis and Machine Intelligence*, vol. 20, no. 11, pp. 1254–1259, Nov 1998.

[2] D. Gao and N. Vasconcelos, "Bottom-up saliency is a discriminant process," in *2007 IEEE 11th International Conference on Computer Vision*, Oct 2007, pp. 1–6.

[3] D. Gao, V. Mahadevan, and N. Vasconcelos, "On the plausibility of the discriminant center-surround hypothesis for visual saliency," *Journal of Vision*, vol. 8, no. 7, pp. 1–18, 2008.

[4] M. M. Cheng, N. J. Mitra, X. Huang, P. H. S. Torr, and S. M. Hu, "Global contrast based salient region detection," *IEEE Transactions on Pattern Analysis and Machine Intelligence*, vol. 37, no. 3, pp. 569–582, March 2015.

[5] F. Perazzi, P. Krhenbhl, Y. Pritch, and A. Hornung, "Saliency filters: Contrast based filtering for salient region detection," in *2012 IEEE Conference on Computer Vision and Pattern Recognition*, June 2012, pp. 733–740.

[6] B. Schlkopf, J. Platt, and T. Hofmann, *Graph-Based Visual Saliency*. MIT Press, 2007, pp. 545–552. [Online]. Available: http://ieeexplore.ieee.org/xpl/articleDetails.jsp?arnumber=6287326

[7] C. Yang, L. Zhang, H. Lu, X. Ruan, and M. H. Yang, "Saliency detection via graph-based manifold ranking," in *2013 IEEE Conference on Computer Vision and Pattern Recognition*, June 2013, pp. 3166–3173.

[8] C. Gong, D. Tao, W. Liu, S. J. Maybank, M. Fang, K. Fu, and J. Yang, "Saliency propagation from simple to difficult," in *2015 IEEE Conference on Computer Vision and Pattern Recognition (CVPR)*, June 2015, pp. 2531–2539.

[9] K. Fu, C. Gong, I. Y. H. Gu, and J. Yang, "Normalized cut-based saliency detection by adaptive multi-level region merging," *IEEE Transactions on Image Processing*, vol. 24, no. 12, pp. 5671–5683, Dec 2015.

[10] Y. Zhang, G. Jiang, M. Yu, and K. Chen, "Stereoscopic visual attention model for 3d video," in *International Conference on Advances in Multimedia Modeling*, 2010, pp. 314–324.

[11] C. Chamaret, S. Godeffroy, P. Lopez, and O. L. Meur, "Adaptive 3d rendering based on region-of-interest," *Proceedings of SPIE - The International Society for Optical Engineering*, vol. 7524, 2010.

[12] Y. Niu, Y. Geng, X. Li, and F. Liu, "Leveraging stereopsis for saliency analysis," in *2012 IEEE Conference on Computer Vision and Pattern Recognition*, June 2012, pp. 454–461.

[13] Y. Fang, J. Wang, M. Narwaria, P. L. Callet, and W. Lin, "Saliency detection for stereoscopic images," *IEEE Transactions on Image Processing*, vol. 23, no. 6, pp. 2625–2636, June 2014.

[14] H. Peng, B. Li, W. Xiong, W. Hu, and R. Ji, "Rgbd salient object detection: A benchmark and algorithms," *National Laboratory of Pattern Recognition*, vol. 8691, pp. 92–109, 2014.

[15] H. Song, Z. Liu, H. Du, G. Sun, O. L. Meur, and T. Ren, "Depth-aware salient object detection and segmentation via multiscale discriminative saliency fusion and bootstrap learning," *IEEE Transactions on Image Processing*, vol. 26, no. 9, pp. 4204–4216, Sept 2017.

[16] L. Ferreira, L. A. da Silva Cruz, and P. Assuncao, "A method to compute saliency regions in 3d video based on fusion of feature maps," in *2015 IEEE International Conference on Multimedia and Expo (ICME)*, June 2015, pp. 1–6.

[17] Z. Liu, X. Zhang, S. Luo, and O. L. Meur, "Superpixel-based spatiotemporal saliency detection," *IEEE Transactions on Circuits and Systems for Video Technology*, vol. 24, no. 9, pp. 1522–1540, Sept 2014.

[18] K. Fu, I. Y. H. Gu, Y. Yun, C. Gong, and J. Yang, "Graph construction for salient object detection in videos," in *2014 22nd International Conference on Pattern Recognition*, Aug 2014, pp. 2371–2376.

[19] Z. Liu, J. Li, L. Ye, G. Sun, and L. Shen, "Saliency detection for unconstrained videos using superpixel-level graph and spatiotemporal propagation," *IEEE Transactions on Circuits and Systems for Video Technology*, vol. 27, no. 12, pp. 2527–2542, Dec 2017.

[20] X. Zhou, Z. Liu, C. Gong, and W. Liu, "Improving video saliency detection via localized estimation and spatiotemporal refinement," *IEEE Transactions on Multimedia*, pp. 1–1, 2018.

[21] A. Krizhevsky, I. Sutskever, and G. E. Hinton, "Imagenet classification with deep convolutional neural networks," in *International Conference on Neural Information Processing Systems*, 2012, pp. 1097–1105.

[22] J. Deng, W. Dong, R. Socher, L. J. Li, K. Li, and L. Fei-Fei, "Imagenet: A large-scale hierarchical image database," in *2009 IEEE Conference on Computer Vision and Pattern Recognition*, June 2009, pp. 248–255.

[23] G. Li and Y. Yu, "Visual saliency based on multiscale deep features," in *Computer Vision and Pattern Recognition*, 2015, pp. 5455–5463.

[24] R. Zhao, W. Ouyang, H. Li, and X. Wang, "Saliency detection by multi-context deep learning," in *2015 IEEE Conference on Computer Vision and Pattern Recognition (CVPR)*, June 2015, pp. 1265–1274.

[25] W. Wang, J. Shen, and L. Shao, "Video salient object detection via fully convolutional networks," *IEEE Transactions on Image Processing*, vol. 27, no. 1, pp. 38–49, Jan 2018.

[26] C. Zach, T. Pock, and H. Bischof, "A duality based approach for realtime tv-l 1 optical flow," *Pattern Recognition*, pp. 214–223, 2007.

[27] J. S. Pérez, E. Meinhardt-Llopis, and G. Facciolo, "Tv-l1 optical flow estimation," *Image Processing On Line*, vol. 2013, pp. 137–150, 2013.

[28] K. Mller, H. Schwarz, D. Marpe, C. Bartnik, S. Bosse, H. Brust, T. Hinz, H. Lakshman, P. Merkle, F. H. Rhee, G. Tech, M. Winken, and T. Wiegand, "3d high-efficiency video coding for multi-view video and depth data," *IEEE Transactions on Image Processing*, vol. 22, no. 9, pp. 3366–3378, Sept 2013.

[29] M. Urvoy, M. Barkowsky, R. Cousseau, Y. Koudota, V. Ricorde, P. L. Callet, J. Gutirrez, and N. Garca, "Nama3ds1-cospad1: Subjective video quality assessment database on coding conditions introducing freely available high quality 3d stereoscopic sequences," in *2012 Fourth International Workshop on Quality of Multimedia Experience*, July 2012, pp. 109–114.

[30] B. Scholkopf, J. Platt, and T. Hofmann, *Graph-Based Visual Saliency*. MIT Press, 2007, pp. 545–552. [Online]. Available: http://ieeexplore.ieee.org/xpl/articleDetails.jsp?arnumber=6287326

[31] R. Achanta, S. Hemami, F. Estrada, and S. Susstrunk, "Frequency-tuned salient region detection," in *2009 IEEE Conference on Computer Vision and Pattern Recognition*, June 2009, pp. 1597–1604.

[32] C. Yang, L. Zhang, and H. Lu, "Graph-regularized saliency detection with convex-hull-based center prior," *IEEE Signal Processing Letters*, vol. 20, no. 7, pp. 637–640, July 2013.

[33] L. Wang, L. Wang, H. Lu, P. Zhang, and X. Ruan, "Saliency detection with recurrent fully convolutional networks," in *European Conference on Computer Vision*. Springer, 2016, pp. 825–841.

[34] W. Wang, J. Shen, and F. Porikli, "Saliency-aware geodesic video object segmentation," in *2015 IEEE Conference on Computer Vision and Pattern Recognition*, June 2015, pp. 3395–3402.